J Physiol 599.12 (2021) pp 3151–3167

The Journal of Physiology

The subiculum sensitizes retrosplenial cortex layer 2/3 pyramidal neurons

Mengxuan Gao[1], Asako Noguchi[1] and Yuji Ikegaya[1,2,3]

[1] *Graduate School of Pharmaceutical Sciences, The University of Tokyo, Tokyo, 113-0033, Japan*
[2] *Institute of AI and Beyond, The University of Tokyo, Tokyo, 113-0033, Japan*
[3] *Center for Information and Neural Networks, National Institute of Information and Communications Technology, Suita City, Osaka, 565–0871, Japan*

Edited by: Katalin Toth & Jean-Claude Béïque

Key points

- Neurons in the retrosplenial cortex (RSC), a cerebral region that connects synaptically with various brain regions, are known to increase neuronal activity in accordance with hippocampal sharp wave-ripples.
- Pyramidal cells in granular RSC (gRSC) layer 2/3, but not layer 5, exhibit slowly ramping depolarization and considerably delayed spikes in response to a step-pulse current injection.
- The latencies of delayed spikes in RSC layer 2/3 pyramidal neurons were shortened by a preceding current injection.
- This effect was mimicked by activation of axonal afferents from the subiculum, but not of neocortical afferents.
- The subiculum is likely to facilitate information processing and flow in the RSC.

Abstract The retrosplenial cortex (RSC), a cerebral region involved in diverse cognitive functions, is an anatomical hub that forms monosynaptic connections with various brain areas. Here, we report a unique form of short-term intrinsic plasticity in mouse granular RSC layer 2/3 pyramidal cells. These cells exhibited delayed spikes in response to somatic current injection, but the spike latencies were shortened by a preceding brief depolarization (priming). This priming-induced sensitization is distinct from desensitization, which is commonly observed in other cortical neurons. The facilitatory priming effect lasted for more than 3 s, providing a time window for increased sensitivity to RSC inputs. Based on *in vitro* and *in vivo* patch-clamp recordings following optogenetic stimulation of axonal fibres, we found that preactivation of subicular afferents replicated the facilitatory priming effect. The results suggest that subicular inputs to RSC layer 2/3 neurons may modulate subsequent information integration in the RSC layer 2/3 circuits.

(Received 24 November 2020; accepted after revision 13 April 2021; first published online 20 April 2021)
Corresponding author Y. Ikegaya: Laboratory of Chemical Pharmacology, Graduate School of Pharmaceutical Sciences, The University of Tokyo, 7-3-1 Hongo, Bunkyo-ku, Tokyo 113-0033, Japan. Email: yuji@ikegaya.jp

Mengxuan Gao graduated from the Graduate School of Pharmaceutical Sciences in The University of Tokyo. She received a master's degree in 2018 and a doctor's degree in 2021. Her research mainly focused on neuronal activities of the hippocampal and cortical areas using electrophysiological recording techniques.

DOI: 10.1113/JP281152

Introduction

The retrosplenial cortex (RSC) is involved in multiple cognitive functions, including spatial navigation, sensory information processing, episodic memory, and imagination of future events (Vann *et al.* 2003, 2009; Czajkowski *et al.* 2014). The RSC contains place cells (Mao *et al.* 2017) and head-direction cells (Chen *et al.* 1994) and acts as a neural hub of spatial signal processing (Alexander & Nitz, 2017). Lesion or inactivation of the RSC impairs performance in contextual fear conditioning (Keene & Bucci, 2008; Corcoran *et al.* 2011) and encoding of history- and value-related information (Hattori *et al.* 2019).

These multifaceted functions of the RSC are consistent with anatomical evidence; the RSC makes synaptic connections with a variety of cortical and subcortical brain structures, including the subiculum, the parietal cortex, the prefrontal cortex, and the limbic thalamus (Vann *et al.* 2009). This unique connectivity implies that the RSC integrates and transforms different types of information in allocentric and egocentric frameworks (Alexander & Nitz, 2015; Nixima *et al.* 2017), which are associated with the signal of place cells and grid cells (Alexander & Nitz, 2017). Consistent with this notion, recent evidence has demonstrated that the RSC relays hippocampal information to the neocortex during sharp-wave ripples (SWRs), high-frequency oscillations that contribute to memory consolidation during behavioural immobility and slow-wave sleep (Nitzan *et al.* 2020; Opalka *et al.* 2020).

Despite the roles of the RSC in hippocampocortical communications, the basic electrophysiological nature of RSC neurons remains unclear. It has been reported that hippocampal SWRs cause layer-dependent neuronal responses in the granular RSC (gRSC) (Nitzan *et al.* 2020). The intrinsic properties of pyramidal cells are also layer-specific; pyramidal cells in gRSC layer 2/3 (L2/3), but not gRSC layer 5 (L5), exhibit slowly ramping depolarization and considerably delayed spikes in response to a step-pulse current injection (Kurotani *et al.* 2013). The late spikes are reported to be shaped by the potassium channels Kv1.1, Kv1.4 and Kv4.3. Late-spiking neurons can respond to persistent burst inputs with high reliability and precision, which may allow them to encode subicular head-direction inputs (Brennan *et al.* 2020). Here, we show that the timing of the late spikes in gRSC L2/3 pyramidal neurons is influenced by preceding activation of the subiculum.

Methods

Ethical approval

Animal experiments were performed with the approval of the Animal Experiment Ethics Committee at the University of Tokyo (approval number: P24-8, P29-9) and according to the University of Tokyo guidelines for the care and use of laboratory animals. These experimental protocols were performed in accordance with the *Fundamental Guidelines for Proper Conduct of Animal Experiment and Related Activities in Academic Research Institutions* (Ministry of Education, Culture, Sports, Science and Technology, Notice No. 71 of 2006), the *Standards for Breeding and Housing of and Pain Alleviation for Experimental Animals* (Ministry of the Environment, Notice No. 88 of 2006) and the *Guidelines on the Method of Animal Disposal* (Prime Minister's Office, Notice No. 40 of 1995). All animals were housed on a 12/12 h dark-light cycle (lights on from 07.00 to 19.00) at 22 ± 1°C with food and water provided *ad libitum*.

Inhibitors

Dendrotoxin-K (DTX-K) was purchased from Sigma-Aldrich (St Louis, MO, USA). 6-cyano-7-nitroquinoxaline-6,7-dinitroquinoxaline-2,3-dione (DNQX) and D-2-amino-5-phosphonopentanoic acid (D-AP5) were purchased from Tocris Bioscience (Bristol, UK). Picrotoxin was purchased from Fujifilm Wako Pure Chemical Corporation (Tokyo, Japan).

Slice preparation

Acute slices were prepared from the hippocampi of 3- to 5-week-old ICR mice of both sexes (SLC, Shizuoka, Japan). The mice were briefly anaesthetized with isoflurane and decapitated. The brains were removed and placed in an ice-cold oxygenated solution containing the following (in mM): 27 $NaHCO_3$, 1.5 NaH_2PO_4, 2.5 KCl, 0.5 ascorbic acid, 1 $CaCl_2$, 7 $MgSO_4$, and 222.1 sucrose. Coronal brain blocks containing the granule retrosplenial cortex formation were sliced at a thickness of 400 μm at a speed of 0.08 mm/s using a Leica vibratome (VT1200S, Leica Microsystems, Nussloch, Germany). The slices were left to recover at 35°C for at least 20 min in oxygenated artificial cerebrospinal fluid (aCSF) containing the following (in mM): 127 NaCl, 26 $NaHCO_3$, 1.6 KCl, 1.24 KH_2PO_4, 1.3 $MgSO_4$, 2.4 $CaCl_2$, and 10 glucose.

In vitro electrophysiological recordings

Experiments were performed in a submerged chamber perfused at 7−9 ml/min with oxygenated aCSF at room temperature. Whole-cell patch-clamp recordings were obtained from small pyramidal cells in gRSC L2/3, which were visually identified under infrared differential interference contrast microscopy and were confirmed by their characteristic late-spiking response to somatic current

injection. In response to suprathreshold depolarizing current steps, late-spiking cells typically showed ramp depolarizations and comparatively long delays before spike train onset. Borosilicate glass pipettes (4–7 MΩ) were filled with a potassium-based solution containing the following (in mM): 120 potassium gluconate, 5 KCl, 10 HEPES, 10 disodium phosphocreatine, 2 Mg-ATP, 0.1 Na_2-GTP, 0.2 EGTA and 0.2% biocytin. The signals were amplified and digitized at a sampling rate of 20 kHz using a MultiClamp 700B amplifier and a Digidata 1440A digitizer that were controlled by pCLAMP 10.3 software (Molecular Devices). The liquid junction potentials were automatically corrected before each experiment using the Pipette Offset mode (Molecular Devices) and not corrected *post hoc*. The fast and slow time constants of depolarization induced by current injection were measured using a two-term exponential curve fit: $f(t) = A_{\text{fast}}e^{-t/\tau_{\text{fast}}} + A_{\text{slow}}e^{-t/\tau_{\text{slow}}}$, where τ_{fast} and τ_{slow} represent fast and slow time constants, and A_{fast} and A_{slow} represent the amplitudes of the fast and slow exponential components, respectively. The amplitude ratio of the slow exponential component was calculated as the percentage of A_{slow} to ($A_{\text{fast}} + A_{\text{slow}}$). Extracellular stimulation was applied by a concentric electrode (Unique Medical, USK-25). For optogenetic stimulation, pulses of 473-nm laser light were delivered through a 40× objective lens, and the intensity of light stimulation (0.1–1.5 mW) was adjusted to induce excitatory postsynaptic potentials (EPSPs) with amplitudes of approximately 5 mV. The initiation of an evoked EPSP was defined as the time point when the rising speed of the membrane potential first exceeded 0.1 mV/ms after the illumination onset. After experimental procedures, the brain slices were post-fixed in 4% (w/v) paraformaldehyde (PFA) (Wako) solution for more than 24 h and washed 3 × 10 min by phosphate-buffered saline (PBS (−)) containing the following (in mM): 137 NaCl, 2.68 KCl, 8.1 Na_2HPO_4, 1.47 KH_2PO_4. To visualize the recorded neurons, the slices were then incubated in 2 μg/ml streptavidin-Alexa Fluor 594 conjugate with 0.1 % Triton X-100 in PBS (−) for 4–6 h.

In vivo electrophysiological recordings

Whole-cell recordings were obtained from postnatal day 28 to 40 male ICR mice as previously described (Ishikawa *et al.* 2014; Funayama *et al.* 2015). After being exposed to an enriched environment for 30 min, each mouse was anaesthetized with urethane (2.25 g/kg, I.P.). Anaesthesia was confirmed by a lack of paw withdrawal, whisker movement, and eyeblink reflexes. The skin was subsequently removed from the head, and a metal head fixation plate was implanted. A craniotomy (2.0 × 1.0 mm^2) centred on the point 1.5 mm posterior to the bregma and 1.0 mm ventrolateral to the sagittal suture was performed. The exposed surface was covered with 1.7% agar at a thickness of 1.5 mm. Whole-cell patch-clamp recordings were obtained from neurons in the gRSC (AP: −1.0 to −3.0 mm; ML: 0.5 mm; DV: 0.5–0.9 mm) using borosilicate glass electrodes (4–7 MΩ). Pyramidal cells were identified by their late-spiking properties and by *post hoc* histological analysis. For current-clamp recordings, the intrapipette solution consisted of the following reagents (in mM): 120 potassium gluconate, 5 KCl, 10 HEPES, 10 disodium phosphocreatine, 2 Mg-ATP, 0.1 Na_2-GTP, 0.2 EGTA (pH 7.3), and 0.2% biocytin. Recordings were not corrected *post hoc* for liquid junction potential. Cells were discarded if the mean resting potential was more positive than −55 mV or if the action potentials were below −20 mV. Simultaneous optogenetic stimulation at 3 mW was delivered to the subiculum via an optic fibre, which was implanted into the viral injection site (3.5 mm posterior 2.5 mm lateral to bregma) before patch-clamp recordings. Virus injections were performed 2—3 weeks before the recordings. All signals were digitized at a sampling rate of 20 kHz using a Digidata 1440A digitizer controlled by pCLAMP 10.3 software (Molecular Devices). After recording, mice were perfused with cold PBS (−) followed by 4% PFA, and the brains were quickly removed and placed in 4% PFA for more than 24 h. Brain slices were made by a microtome (DTK-1000N, D.S.K), and the recorded neurons were visualized following the same procedure as *in vitro*.

Virus injection

Mice aged 14–17 days were anaesthetized with xylazine (0.01 ml/g) and pentobarbital (0.005 ml/g, I.P.) or inhalational isoflurane (1.5%), and their heads were fixed in a stereotaxic frame. A craniotomy was performed above the subiculum (3.5 mm posterior and 2.5 mm lateral to bregma) or the gRSC L5 area (2.0 mm posterior and 0.2 mm lateral to bregma). A bevelled glass pipette loaded with adeno-associated virus (AAV5-CaMKIIα-ChR2(H134R)-EYFP, 2.2×10^{12} GC/ml) was unilaterally injected into the subiculum (500 nl, 100 nl/min, 1.5 mm beneath the pia) or the gRSC L5 area (250 nl, 100 nl/min, 0.6 mm deep from the pia). After 2–3 weeks of viral injection, mice were used for experiments.

Data analysis

The data were exported at 20 kHz and processed with custom-made routines in MATLAB R2016a (The MathWorks, Natick, MA, USA). Statistical analysis was performed by Student's *t* test, paired *t* test, Kruskal-Wallis

test followed by Dunn's *post hoc* test or bootstrap test for means. Statistical values are included in the figure legends.

Results

Priming depolarization shortens first-spike latencies in gRSC L2/3 neurons

We obtained *in vitro* whole-cell patch-clamp recordings from gRSC L2/3 small pyramidal cells in mouse brain slices (Fig. 1*A*, left). As reported in previous studies (Kurotani *et al*. 2013), a large portion of these neurons exhibited unique electrophysiological characteristics, including late-spiking responses to a step pulse of depolarizing current injection (Fig. 1*B*), high input resistance (432 ± 146 MΩ, mean ± SD of 89 cells), and low resting membrane potentials (−76.2 ± 5.9 mV, mean ± SD of 89 cells). In the present study, we used late spiking, i.e. ramp depolarization before spike train onset, as a physiological marker of L2/3 small pyramidal cells (Fig. 1*B*) and confirmed their pyramidal cell-like morphology through *post hoc* biocytin-based confocal visualization (Fig. 1*A*, right).

In general, the first-spike latencies of neurons are crucial for information transmission and encoding (Gautrais & Thorpe, 1998; Chase & Young, 2007), and the late spike responses of gRSC L2/3 neurons are believed to contribute to unique synaptic integration (Kurotani *et al*. 2013; Nixima *et al*. 2013, 2017). We first examined whether late-spike latencies are modulated by the history of activity of gRSC L2/3 neurons. After a brief (200-ms) depolarizing current was injected into a current-clamped gRSC L2/3 neuron to evoke a spike (priming), the main (500-ms) depolarizing current was injected (Fig. 1*C*, left). The intensities of the injected currents were set to induce a single action potential during the 200-ms priming stimulus, and the intensities of the main current injection were set to be identical to those of the priming stimulation. In control experiments, only the main current was injected without priming (Fig. 1*C*, left). We alternated 'without (w/o) priming' and 'with (w/) priming' trials. The latencies of the first spikes evoked by the main current injection were significantly shorter in the w/ priming trials than in the w/o priming trials (Fig. 1*C*, right; $n = 10$ trials each; $^{**}P = 8.5 \times 10^{-8}$, Student's t test). We repeated these experiments for a total of eight cells in eight slices and obtained the same results (Fig. 1*D*). In experiments involving current injection, spike times may be determined by two factors of membrane potential: (1) the spike threshold to which a membrane potential must be depolarized to initiate an action potential and (2) the depolarization speed at which the membrane potential reaches the action potential threshold. The priming current injection did not alter either the action potential threshold (Fig. 1*E*). Moreover, the resting membrane potentials immediately before the priming current injection were the same as those before the main current injection in the w/ priming trials (before the priming current: −81.9 ± 7.3 mV; before the main current: −81.9 ± 7.5 mV; mean ± SD summarized from 66 trials from 7 cells; $P = 0.94$, $t_6 = 0.077$, paired t test). In addition, the membrane potentials before the main current injection exhibited no significant difference between w/o and w/ trials (w/o trials: −81.8 ± 7.4 mV; w/ trials: −81.9 ± 7.5 mV; mean ± SD summarized from 66 trials from 7 cells; $P = 0.55$, $t_6 = -0.64$, paired t test). Therefore, the prior baseline of membrane potentials cannot explain the facilitatory effect of the priming effect. Interestingly, the priming effect did not require an action potential. When the priming current was reduced to 80% of the current defined above, which was below the spike threshold, a brief depolarization alone was sufficient to shorten the first-spike latencies (Fig. 1*F*), although the effect was slightly weaker than that of the spike-inducing priming stimulus (Fig. 1*G*). Priming currents with the same conditions occasionally elicited multiple spikes, and priming currents that generated more action potentials produced larger priming effects (Fig. 1*H*). Thus, gRSC L2/3 neurons are sensitized depending on the history of their own depolarization.

To examine the possible mechanism of the priming effect, we conducted bath-application of DTX-K, a potent blocker of Kv1 channels, since the late-spiking property of gRSC L2/3 neurons was reported to be shaped by potassium channels including Kv1.1, Kv1.4 and Kv4.3 (Kurotani *et al*. 2013). We conducted the w/o and w/ priming trials in gRSC L2/3 neurons in ACSF, and then bath-applied ACSF with 5 nM DTX-K for more than 5 min and repeated the priming protocols in the same cells. Durations of the priming and main currents were set to be 100 ms and 500 ms, respectively, and the interval between the current injections was 500 ms. Treatment of DTX-K significantly attenuated the extent of shortening of the first spike latencies, as measured as the percentage of the first spike latencies of w/ priming trials *versus* w/o trials (Fig. 1*I*), although the priming effect remained significant in the presence of DTX-K ($P = 2.9 \times 10^{-3}$, $t_4 = -6.51$, one-sample t test *vs*. 100%). This result indicates that the activity of Kv1 channels may partly serve as a candidate mechanism for the priming effects. We also compared the priming effect obtained in normal ACSF and during the application of blockers of synaptic transmission (10 μM DNQX, 50 μM D-AP5, and 20 μM picrotoxin) (Fig. 1*J*). In both groups, the durations and intensities of the current injection were set to be the same as Fig. 1*C*. Bath treatment with the synaptic transmission inhibitors did not significantly influence the extent of the priming effect.

We characterized the facilitatory effect of the priming current injection on the first-spike latencies of gRSC L2/3

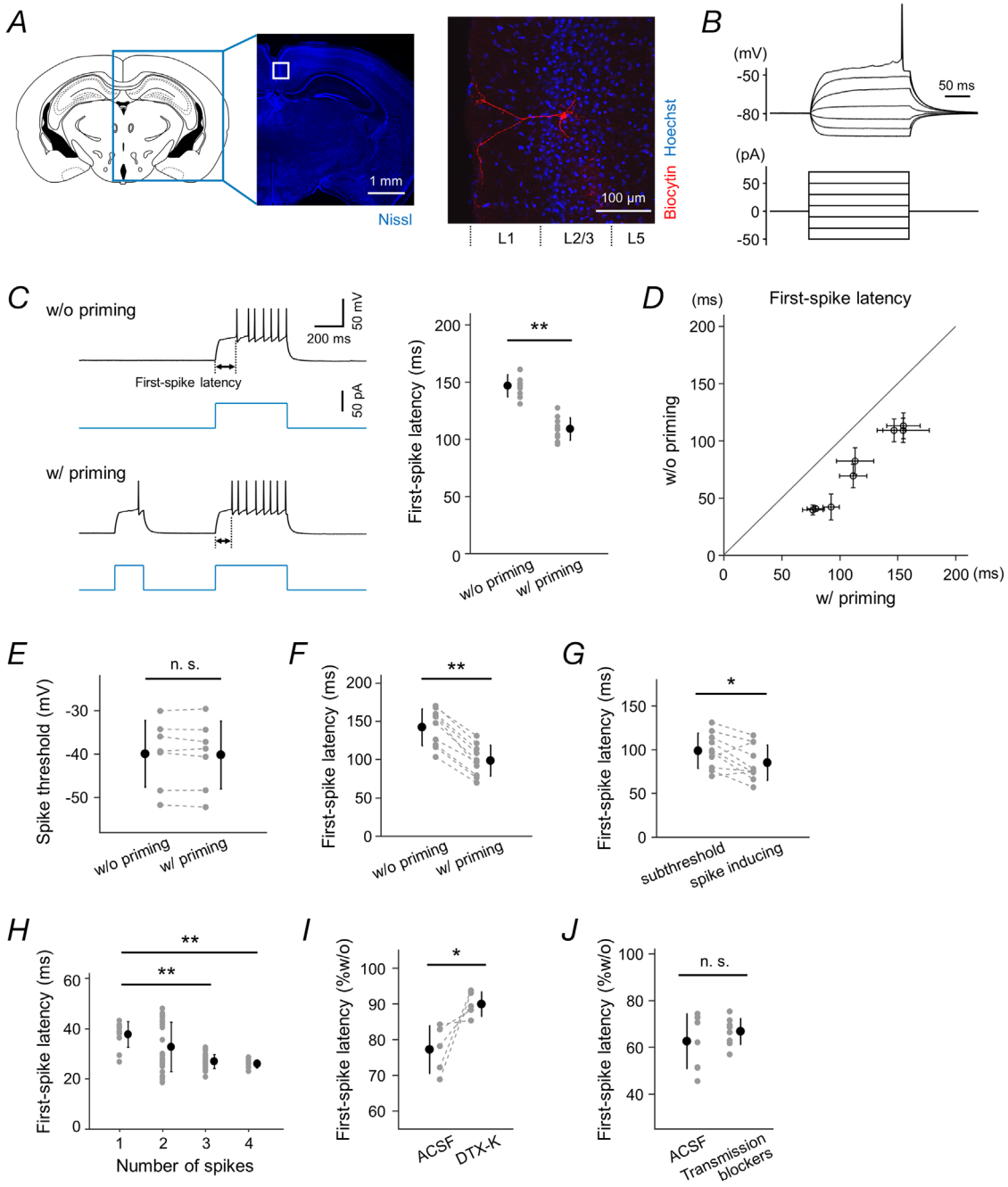

Figure 1. Brief priming depolarization shortens first-spike latency in gRSC L2/3 neurons
A, left: a schematic drawing of a coronal section of the mouse brain and a fluorescence microscopic image of a Nissl-stained brain, in which the white box indicates a recording site (gRSC). *A*, right: representative confocal photograph of a gRSC L2/3 pyramidal cell after biocytin visualization. The recording was conducted using a biocytin-loaded patch-clamp pipette. *B*, voltage responses to step-pulse current injection with different amplitudes ranging from −50 to 70 pA. gRSC L2/3 neurons exhibited a long latency from the onset of current injection to the first evoked spike. *C*, left top: voltage response of a gRSC L2/3 late-spiking neuron to current injection. The current amplitude was set to induce a moderate first-spike latency of approximately 150 ms (w/o priming trial). *C*, left bottom: voltage response of the same neuron to the same current injection but preceded by another depolarizing current injection of the same amplitude (w/ priming trial). *C*, right: first-spike latencies were compared between the w/o and w/ priming trials. The two trial types were alternated for a total of ten trials each. The presence of priming significantly shortened the first-spike latency. The summarized data are presented as the mean ± SD of 10 trials. $^{**}P = 8.5 \times 10^{-8}$, $t_{18} = 8.61$, Student's *t* test, *D*, data from 8 gRSC L2/3 neurons from 3 mice are summarized. The data are presented as the means ± SD of 8–10 trials. $P = 2.3 \times 10^{-7}$, $t_7 = 19.5$, paired *t* test for the average

latencies. *E*, comparison of the spike threshold values between w/o and w/ priming trials. The maximal positive peak in the second derivative of the membrane potential was identified as a spike threshold. There was no significant difference in spike thresholds. Data from 8−10 trials each from 7 gRSC L2/3 neurons from 3 mice are summarized. $P = 0.41$, $t_6 = 0.895$, paired *t* test. *F*, subthreshold priming without spikes shortened the first spike latencies. Data are summarized from 4−11 trials each in 10 gRSC L2/3 neurons from 3 mice. $^{**}P = 2.2 \times 10^{-7}$, $t_9 = 13.9$, paired *t* test. *G*, comparison of the first-spike latency between trials with subthreshold priming and spike-inducing priming. Data from 4−11 trials each from 10 gRSC L2/3 neurons from 3 mice are summarized. $^{*}P = 2.2 \times 10^{-2}$, $t_{9\ =} 2.76$, paired *t* test. *H*, a priming current of the same duration but that induced more spikes had stronger priming effects on first-spike latency. A 200-ms priming current was delivered 50 ms before the following main current. Data from 10 trials each from 9 gRSC L2/3 neurons from 3 mice are summarized. $n = 11$, 32, 37 and 10 trials for groups with 1, 2, 3 and 4 spikes, respectively. *P* values were determined by the Kruskal-Wallis test followed by Dunn's *post hoc* test. $^{**}P = 1.5 \times 10^{-3}$ for group 1 *versus* 3; $^{**}P = 3.0 \times 10^{-3}$ for group 1 *versus* 4. The *P* value was 3.1×10^{-4}, as determined by the Kruskal-Wallis test. *I*, comparison of the priming effect in ACSF and during bath-perfusion with 5 nM DTX-K. The extent of the priming effect was measured as the percentage of first-spike latencies in w/ priming trials to those in w/o trials in each group. The priming current was 100 ms in duration. Data points of the same cells are connected by dashed lines. Data are summarized from 4–10 trials each in 5 gRSC L2/3 neurons from 5 mice. $^{*}P = 4.7 \times 10^{-2}$, $t_4 = -2.84$, paired *t* test. *J*, comparison of the priming effect in ACSF and during bath application of blockers of synaptic transmission (10 μM DNQX, 50 μM D-AP5, and 20 μM picrotoxin). The priming current was 200 ms in duration. Data are summarized from 7–10 trials each in 8 and 9 gRSC L2/3 neurons from 3 mice, respectively. $P = 0.35$, $t_{15} = -0.97$, Student's *t* test. [Colour figure can be viewed at wileyonlinelibrary.com]

neurons by modifying three parameters of the priming current injection: (1) the interval period between the offset time of the priming current injection and the onset time of the main current stimulation (interval), (2) the duration of the priming current injection (duration), and (3) the amplitudes of the priming current (strength) (Fig. 2*A*). To control the experimental conditions, we changed one parameter while keeping the other two parameters constant. Specifically, the interval, duration, and strength were set to 50 ms, 200 ms, and 100%, respectively, unless otherwise specified; note that the strength represents the percentage of the priming current amplitude to the main current amplitude. The strength was normalized to 100% before data pooling because it was optimized to produce a single action potential during the priming current injection for each cell; the mean amplitude of the priming current was 94 ± 8 pA (mean ± SEM of 18 cells). In each experimental cycle, different conditions for the priming current injection were tested in mixed orders. In the interval range of 50 ms to 3 s, shorter intervals caused shorter first-spike latencies in gRSC L2/3 neurons (Fig. 2*B*). The mean interval to produce 50% of the maximal facilitatory effect was 316 ± 156 ms (mean ± SD of 10 cells). In the range of durations between 50 and 300 ms, longer durations caused shorter first-spike latencies, but the priming effect became saturated at a duration of approximately 100 ms (Fig. 2*C*). The strength was examined in the range of −100% and 120%, where negative values indicate hyperpolarizing currents and zero represents w/o priming trials. Only depolarizing currents shortened the first-spike latencies, while hyperpolarizing currents failed to affect the first-spike latencies (Fig. 2*D*).

Using a two-term exponential curve fit, we compared the time constants during the depolarization induced by the main stimulation for the w/o and w/ priming trials (Fig. 3*A*; root mean square error = 2.53 ± 1.22, mean ± SD of 123 trials from 7 cells). The fast time constants (τ_{fast}) were not significantly different between the two groups (Fig. 3*B*). However, the slow time constants (τ_{slow}) were significantly decreased by the priming current injection, although the amplitude ratios of the slow component were not significantly changed (Fig. 3*C*). Thus, in response to the main stimulation, the slow time constant serves as a critical factor in shortening the spike latencies. We next injected a brief ramp current instead of a step current as the main stimulation to investigate the minimum current intensity that was necessary to induce spikes in gRSC L2/3 neurons (Fig. 3*D*). The duration of the ramp current injection was set to 50 ms. The ramp current was of increasing intensity from 0 to about 250 pA (277 ± 44 pA, mean ± SD of 10 cells) to evoke 2−3 spikes. In w/ priming trials, the intensities of the priming current were set to induce a single action potential during the 200-ms stimulus (84.5 ± 22.5 pA, mean ± SD of 10 cells), and the interval between the current injections was set to 500 ms. The spike timing in w/o priming trials tended to be more delayed than the w/ trials (Fig. 3*D*, inset). During the ramp current injection, timing of the maximal positive peak in the second derivative of the membrane potential was identified as the initiation of the first spike. Based on the timing of spike initiation, we measured the minimum current intensity that could evoke the first spike as a threshold intensity and compared the intensities for w/o and w/ priming trials (Fig. 3*E*). The threshold intensities are significantly lower in w/ priming trials, suggesting that the spike response was facilitated by the priming stimulation in gRSC L2/3.

We also monitored the input resistances of gRSC L2/3 neurons by injecting brief hyperpolarizing step currents (−50 pA for 50 ms) 50 ms before the priming and main depolarizing current injections (Fig. 4). The interval between the offset time of the priming current and the onset time of the main current was set as 200, 500,

or 1000 ms (Fig. 4*A*). The input resistance was calculated as $\Delta V/I$, where ΔV and I represent the membrane potential change caused by a hyperpolarizing step current and the step current magnitude (herein, $I = -50$ pA). No significant change was found before and after the priming current (Fig. 4*B*), and the input resistance was not significantly correlated with the first spike latency during the main current injection (Fig. 4*C*, Table S1).

To determine whether facilitatory priming effects are a common phenomenon in the brain, we examined four other types of pyramidal cells in L5 of the gRSC, L2/3 of the anterior cingulate cortex (ACC), the hippocampal CA1 area and L6 of the perirhinal cortex (PRC) using the same experimental protocol with three parameters (Fig. 5). The amplitudes of the current injection were set to induce spikes after a latency of approximately 100 ms; the

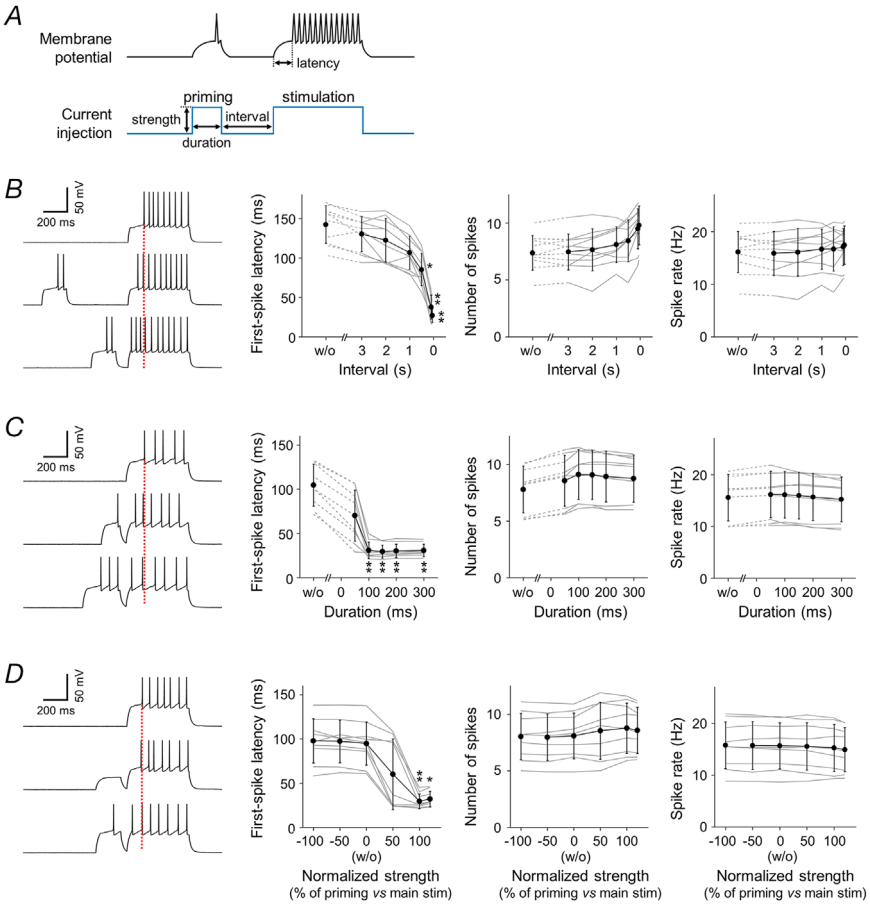

Figure 2. Characterization of priming-induced sensitization in gRSC L2/3 neurons
A, schematic illustration of the three parameters tested in the experiments. The priming procedure is a current injection procedure prior to the main current injection ('stimulation') for which first-spike latencies were measured. Unless otherwise specified, the interval and duration were set as 50 ms and 200 ms, respectively. For each cell, the strength of stimulation was optimized so that the neurons fired a single action potential during a 200-ms priming current injection, and this strength was normalized to 100%. *B*, representative traces (left) are shown. First-spike latencies (middle left), spike numbers (middle right), and spike rates during current injection (right) were measured for different intervals. The data are presented as the mean ± SD of 10 cells from 3 mice (4–11 trials per cell). The Kruskal-Wallis test was followed by Dunn's *post hoc* test. $P = 9.7\times10^{-10}$ (middle left), 1.3×10^{-2} (middle right) and 0.97 (right), as determined by the Kruskal-Wallis test. The results of Dunn's test compared to the control (w/o priming trials) are indicated above the data points. $^{*}P < 0.05$, $^{**}P < 0.01$. *C* and *D*, the same as *B*, measured after different durations (*C*) or strengths (*D*) of priming currents. In the *x*-axis in the panel *D*, the strength of the priming stimulation is shown as the percentage of priming current amplitude to the main current amplitude. Negative values represent hyperpolarizing currents, whereas zero represents w/o trials. The data are presented as the means ± SD of 9 cells from 4 mice (10 trials per cell). $P = 1.6\times10^{-5}$ (middle left), 0.43 (middle right) and 0.84 (right) in *C*; $P = 6.2\times10^{-6}$ (middle left), 0.93 (middle right) and 0.99 (right) in *D*), as determined by the Kruskal-Wallis test. The results of Dunn's test compared to the control (in *C*, w/o priming trials; in *D*, trials with the priming current strength = 0) are indicated above the data points. $^{*}P < 0.05$, $^{**}P < 0.01$. [Colour figure can be viewed at wileyonlinelibrary.com]

mean currents were 98 ± 5 pA for gRSC L5, 124 ± 10 pA for ACC L2/3, 54 ± 3 pA for the hippocampal CA1 region and 85 ± 5 pA for PRC L6 (means ± SEMs of 8, 9, 9 and 11 cells, respectively). In all pyramidal cells, the priming effect was in contrast to that observed in gRSC L2/3 neurons (except for one late-spiking cell in PRC L6): the priming current injection tended to prolong the first-spike latencies. These results suggest that pyramidal cells are basically self-desensitized upon preceding excitation. In general, such autosuppression is thought to act as a negative feedback mechanism that protects the operation of the system against over-excitement (Ha & Cheong, 2017). Another important difference is that the suppressive priming effect persisted for only a short time; it disappeared within 150 ms of the priming current injection.

The low resting membrane potentials of gRSC L2/3 neurons are distinct from the other neuron types. We examined whether the facilitatory priming effect is induced in other neurons when their membrane voltages were hyperpolarized. We applied the priming protocols (same as in Fig. 1*C*) to gRSC L5 under the normal condition in which no current was injected except for the priming and main stimuli (Fig. 6*A*) and under the hyperpolarized condition in which a hyperpolarizing current was constantly injected into the neurons to maintain their membrane potentials more negative than −75 mV (Fig. 6*B*). The resting membrane potentials of gRSC L5 neurons were −67.1 ± 0.8 mV under the normal condition (mean ± SD of 6 cells) and −79.6 ± 3.0 mV under the hyperpolarized condition (mean ± SD of 8 cells). No significant priming effect was induced under either of the conditions, suggesting that low membrane potentials cannot account for the priming effect.

Optogenetic activation of subicular axons mimics facilitatory priming effects

In the experiments above, we injected artificial electrical currents into cell bodies as priming stimuli. We wondered

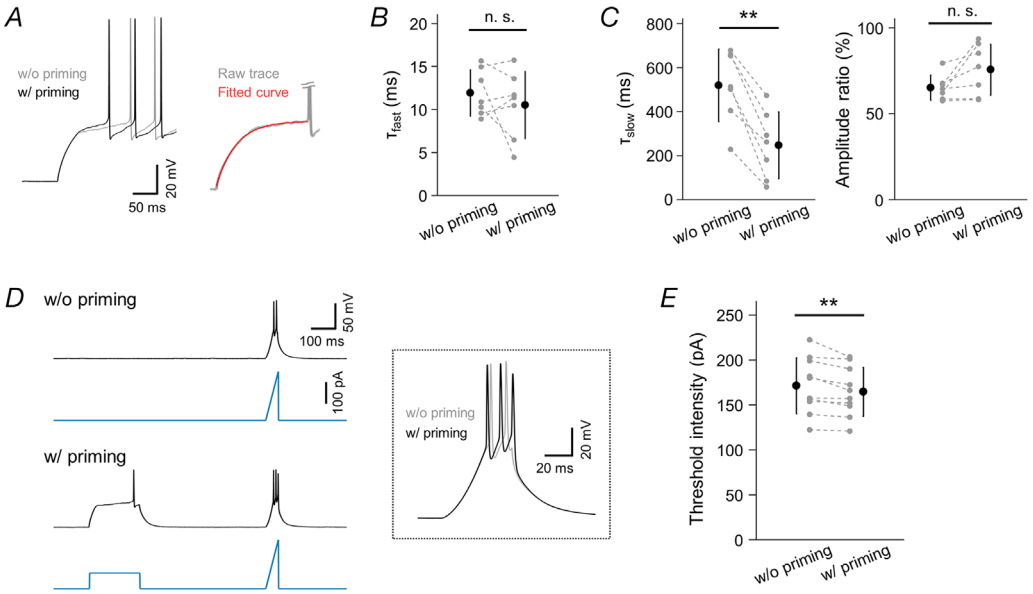

Figure 3. Priming current injection decreases the slow time constant of depolarization and lowers the necessary spiking threshold intensity
A, left: representative membrane voltage responses to current injection for w/o priming (grey) or w/ priming (black) trials. The two traces overlapped in an early rising phase. *A*, right: an example trace (grey) and the fitted curve with a two-term exponential model (red). The function of the fitted curve was $f(t) = A_{fast}e^{-t/\tau_{fast}} + A_{slow}e^{-t/\tau_{slow}}B$, comparison of fast time constants (τ_{fast}) between w/o and w/ priming trials. Data are summarized from 7 gRSC L2/3 neurons from 3 mice (4–10 trials per cell). $P = 0.38$, $t_6 = -0.948$, paired *t* test. *C*, left: same as *B*, but for the slow time constants (τ_{slow}). $^{**}P = 5.0 \times 10^{-4}$, $t_6 = -6.80$, paired *t* test. *C*, right: comparison of the amplitude ratios of the slow exponential component calculated as the percentage of A_{slow} to (A_{fast}+A_{slow}). $P = 6.2 \times 10^{-2}$, $t_6 = 2.29$, paired *t* test. *D*, top: voltage response of a gRSC L2/3 late-spiking neuron to a brief ramp current injection. The current was of increasing intensity, and the amplitude was set to evoke 2–3 spikes during the 50-ms stimulus (w/o priming trial). *D*, bottom: voltage response of the same neuron to the same current injection after a priming current injection (w/ priming trial). Inset, the membrane voltage responses to the ramp current injection for w/o priming (grey) or w/ priming (black) trials. *E*, comparison of the minimum current intensity (threshold intensity) to evoke the first spike during the ramp current injection. Data from 10 gRSC L2/3 neurons from 3 mice (6–10 trials per cell) are summarized. Data points of the same cells are connected with dashed lines. $^{**}P = 9.0 \times 10^{-3}$, $t_9 = 3.32$, paired *t* test. [Colour figure can be viewed at wileyonlinelibrary.com]

whether synaptic activation by stimulation of afferent fibres but not somatic injection of currents would produce a similar priming effect in gRSC L2/3 neurons. We selected two upstream brain areas that project to gRSC L2/3 neurons, namely, the dorsal subiculum (Cembrowski *et al.* 2018; Yamawaki *et al.* 2019*a*) and gRSC L5. We injected AAV5-CaMKII-ChR2-EYFP into one of the two areas (Fig. 7*A* and *D*). After 2 weeks, we prepared brain slices and investigated ChR2-expressing axons using a confocal microscope. ChR2-EYFP signal was found in gRSC L2/3 of mice that had received AAV injection into the subiculum (Fig. 7*B* and *C*) and in gRSC L1 and L5 of mice that had received AAV injection into gRSC L5 (Fig. 7*E* and *F*).

We investigated the priming effect of optogenetic stimulation of these ChR2-expressing axons on the first-spike latencies of gRSC L2/3 neurons. We illuminated slices with 2-ms blue light pulses through a 40× objective lens 500 ms or 1 s before the 500-ms main current injection. The light intensity was set to evoke EPSPs with amplitudes of approximately 5 mV (which was nearly maximal under our illumination conditions). The latencies from the illumination onset to the initiation of the evoked EPSPs were 3.9 ± 0.5 ms for subicular inputs and 3.6 ± 0.6 ms for gRSC L5 inputs (mean ± SEM of 6 cells each). Compared to no priming, activation of subicular projections at an interval of 500 ms, but not 1 s, reduced first-spike latencies (Fig. 8*A* and *B*). Thus, optogenetic priming of subicular afferents mimicked the facilitatory priming effect of the brief somatic current injection. When priming stimulation by illumination and priming stimulation by 200-ms somatic current injection were alternated in the same cells, the optical priming induced significantly smaller effects than the current injection (Fig. 8*C*), possibly because the current injection directly stimulated the soma and caused larger membrane potential changes with a spike. On the other hand, the priming of gRSC L5 was suppressive, prolonging the first-spike latencies (Fig. 8*D* and *E*); however, a facilitatory effect was observed when slices were perfused with 10 μM CGP52432, a $GABA_B$ receptor antagonist (Fig. 8*F*). We speculate that endogenous synaptic inputs from the subiculum and gRSC L5 shorten the first-spike latencies in gRSC L2/3 neurons but that the facilitatory effect of gRSC L5 priming is masked by $GABA_B$ receptor activity under normal conditions.

Subicular priming enhances spiking and synaptic responses of gRSC L2/3 neurons

We examined whether optogenetic subicular priming also modulates the responses of gRSC L2/3 neurons to subsequent synaptic activation. A concentric stimulating electrode was placed deeper in the gRSC L2/3 areas than the patch-clamped gRSC L2/3 neurons (Fig. 9*A*). For each cell, the stimulation intensity of a single 50-μs electrical pulse was set to induce a spike with a probability of approximately 40% (ranging between 20 and 60%); note that stimulation at the same intensity induced either a spike or an EPSP in the same cell. The mean spike latency was 4.3 ± 0.6 ms, and the mean half-width of the spikes was 1.60 ± 0.03 ms (mean ± SEM of 277 trials in 17 cells). Thus, the spikes were likely to be synaptically initiated by the stimulation, but it did not reflect an antidromically arrived spike. The field stimulation was delivered 500 ms after optogenetic priming of subicular axons (Fig. 9*B*, left), and the w/ and w/o priming trials were repeated alternatively. The electrical pulse after optogenetic priming increased the firing probability (Fig. 9*B* and *C*). The same procedures were also conducted for brain slices prepared from mice that had received AAV injection into the gRSC L5 inputs (Fig. 9*D*), and

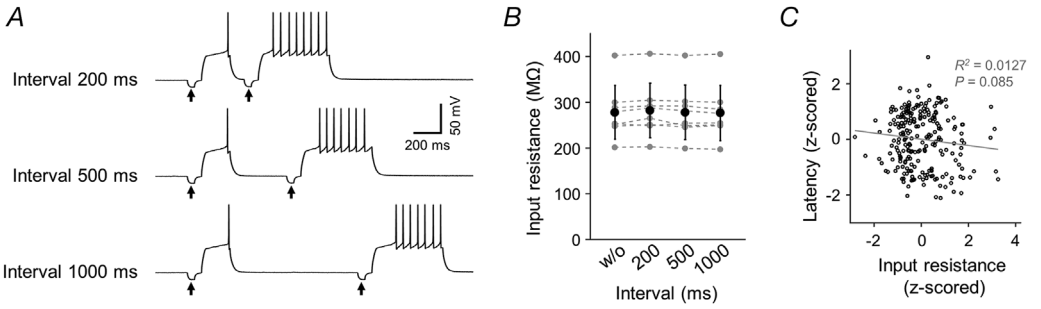

Figure 4. Priming current injection does not affect input resistance
A, example traces of three trials at different intervals (200, 500, or 1000 ms). An input resistance test was conducted before each depolarizing current injection (arrows). The input resistance was measured by a hyperpolarizing current injection of −50 pA for 50 ms conducted 50 ms before each depolarizing current. *B*, comparison of input resistances before (w/o) and after the priming current at different intervals. n = 8 cells (4–6 trials for each interval for each cell). P values were determined by the Kruskal-Wallis test followed by Dunn's *post hoc* test. P = 0.96, as determined by the Kruskal-Wallis test. *C*, the first-spike latencies after various priming current injections were plotted against the input resistance after priming. n = 8 cells. The data were z-standardized with 24–36 data points from each cell.

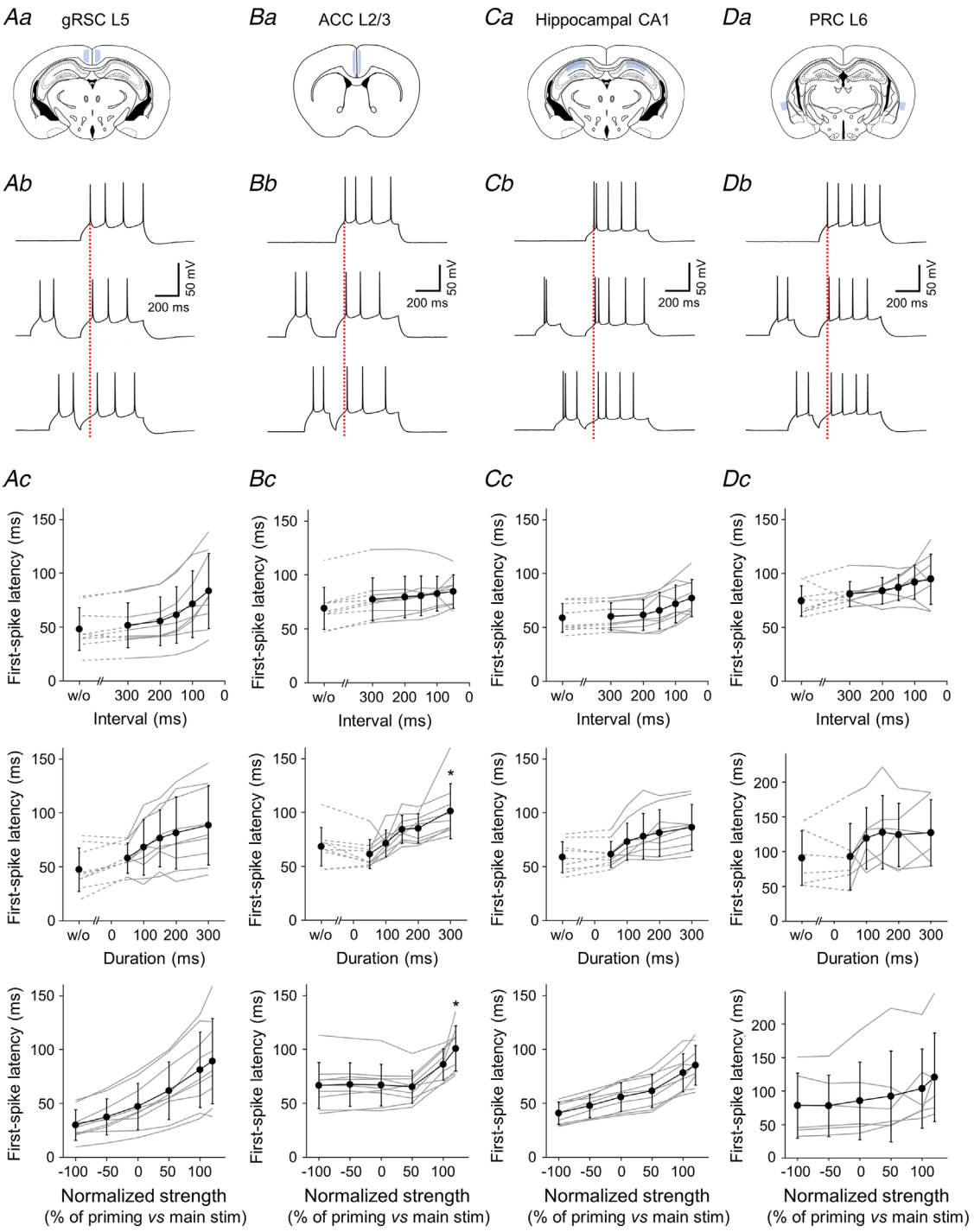

Figure 5. Priming effects in different types of neurons
A, first-spike latencies were measured at different conditions in pyramidal neurons from gRSC L5. *Aa*, location of the measured area in a brain slice. *Ab*, example traces of a trial without priming (top) and a trial with a 200-ms priming current injection at an interval of 200 ms (middle) or an interval of 50 ms (bottom) in the same cell. The time of the first spike in the w/o trial is indicated by the red dotted line. *Ac*, first-spike latencies during main current injection were measured for different intervals (top), durations (middle) and priming current strengths (bottom). The data are presented as the mean ± SD of 9 cells from 6 mice (10 trials per cell). The Kruskal-Wallis test was followed by Dunn's *post hoc* test. The results of Dunn's test compared to the control (w/o priming trials) are indicated above the data points. $^{*}P < 0.05$, $^{**}P < 0.01$. The *P* values determined by the Kruskal-Wallis test were 0.11 (top), 4.4×10^{-2} (middle), and 3.3×10^{-4} (bottom). *B-D*, the same as *A* but in the anterior cingulate cortex (ACC) L2/3 (*B*), the hippocampal CA1 area (*C*) and the perirhinal cortex (PRC) L6 (*D*). In *B* and *C*, the data

are presented as the means ± SD of 9 cells from 2 or 4 mice (10 trials per cell). In *Bc*, the *P* values determined by the Kruskal-Wallis test were 0.27 (top), 1.2×10^{-4} (middle), and 9.1×10^{-4} (bottom). In *Cc*, the *P* values were 0.12 (top), 2.2×10^{-2} (middle), and 7.3×10^{-4} (bottom). In *D*, the data are presented as the means ± SD of eight cells from 3 mice (top) or 6 cells from 2 mice (middle, bottom) (10 trials per cell). In *Dc*, the *P* values were 0.15 (top), 0.42 (middle), and 0.58 (bottom). [Colour figure can be viewed at wileyonlinelibrary.com]

optogenetic priming reduced the firing probabilities of gRSC L2/3 neurons (Fig. 9*E*). Moreover, the intensity of electrical field stimulation was set to depolarize gRSC L2/3 neurons by approximately 5 mV, and these subthreshold EPSPs were compared between trials w/o and w/ optogenetic priming. Consistent with the results of firing probabilities, the EPSP amplitudes were increased or decreased by optogenetic priming of subicular inputs and gRSC L5 inputs, respectively (Fig. 9*F*).

In these experiments, however, we employed electrical stimulation to evoke EPSPs; thus, we could not rule out the possibility that optogenetic priming-enhanced EPSPs arose from paired-pulse facilitation induced by repeated stimulation of the same presynaptic fibres. We thus recorded excitatory postsynaptic currents (EPSCs) evoked by a pair of blue light pulses. Two pulses of 2-ms light illumination were delivered at an interval of 100, 250, or 500 ms to ChR2-expressing subicular (Fig. 10*A*) or gRSC L5 inputs (Fig. 10*B*). In both cases, we observed a tendency towards paired-pulse depression; the second EPSCs were smaller than the first EPSCs, particularly at an interval of 500 ms. Therefore, paired-pulse light stimulation was not able to reproduce the facilitatory priming effect. These results indicate that subicularly enhanced EPSPs in gRSC L2/3 neurons reflect intersynaptic interplay; that is, activation of subicular inputs to gRSC L2/3 neurons increases their responsiveness to other synaptic inputs.

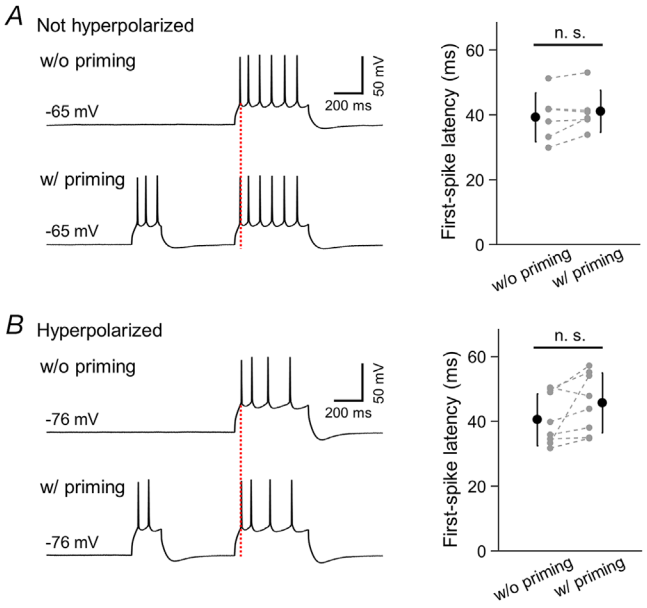

Figure 6. Hyperpolarization of gRSC L5 neurons does not replicate the faciliatory priming effect
A, left: example traces of a trial without priming (top) and with priming (bottom) recorded from a gRSC L5 neuron. Timing of the first spike in the w/o trial is indicated by red dotted line. The durations of the priming and the main current were set to be 200 and 500 ms, respectively, and the interval between the two currents was 500 ms. No current injection was conducted except for the priming and main depolarizing currents. *A*, right: comparison of the first spike latency for trials without priming or with priming. Data points of the same cells are connected by dashed lines. Data are summarized from 6 gRSC L5 neurons from 2 mice (5–8 trials per cell). $P = 0.15$, $t_5 = -1.69$, paired *t* test. *B*, same as *A*, but the membrane potentials were maintained more negative than −75 mV by injecting a hyperpolarizing current, except for the priming and main current. The traces were recorded from the same cell as in *A*. Data are summarized from 8 gRSC L5 neurons of 2 mice (5–11 trials per cell). $P = 7.9 \times 10^{-2}$, $t_7 = -2.06$, paired *t* test. [Colour figure can be viewed at wileyonlinelibrary.com]

Subicular priming augments *in vivo* synaptic activity in gRSC L2/3 neurons

To examine whether the facilitatory effect of optogenetic subicular priming occurs under more physiological conditions, we obtained *in vivo* whole-cell patch-clamp recordings from gRSC L2/3 late-spiking neurons and monitored spontaneous synaptic activity rather than artificially evoked EPSPs (Fig. 11*A*). Mice that had been injected with AAV5-CaMKII-ChR2-EYFP into the dorsal subiculum were anaesthetized with urethane, and an optic fibre was implanted into the injection site (Fig. 11*B*). Then, the gRSC was targeted obliquely, and gRSC L2/3 pyramidal cells were current clamped at 0 pA (Fig. 11*C*). The mean recording time was 748 ± 97 s (mean ± SEM of 5 cells) and ranged from 395 to 940 s. Membrane potential and input resistance were −74.4 ± 3.5 mV and 266.9 ± 31.2 MΩ (mean ± SEM of 5 cells). A 100-ms pulse of blue light was delivered every 5 s through the optic fibre, reliably evoking a postsynaptic potential (PSP) with an amplitude of 22.7 ± 0.3 mV (mean ± SEM of 380 trials in 5 cells) and a mean area under the curve (AUC) of 1.75 ± 0.50 mV s (Fig. 11*D*; mean ± SD of 380 trials in 5 cells). The mean latency from light stimulation onset to the evoked EPSP peak was 65.7 ± 1.4 ms (mean ± SEM of 380 trials in 5 cells). We then focused on the 700-ms periods before (baseline) and after light illumination and calculated the AUC of spontaneous PSPs (Fig. 11*D*, top). The AUCs were significantly greater after subicular priming than during the baseline periods (Fig. 11*E*, Table S2).

Discussion

Although the late spike responses of gRSC L2/3 neurons are thought to be associated with unique synaptic integration (Kurotani *et al.* 2013; Nixima *et al.* 2013, 2017), it is not known whether or how late-spike latencies are modulated in gRSC L2/3 neurons. In the present study, we reported a unique priming effect in gRSC L2/3 late-spiking neurons. Prior depolarization of gRSC L2/3 neurons shortened the latencies of the first action potentials and promoted the spike responses in response

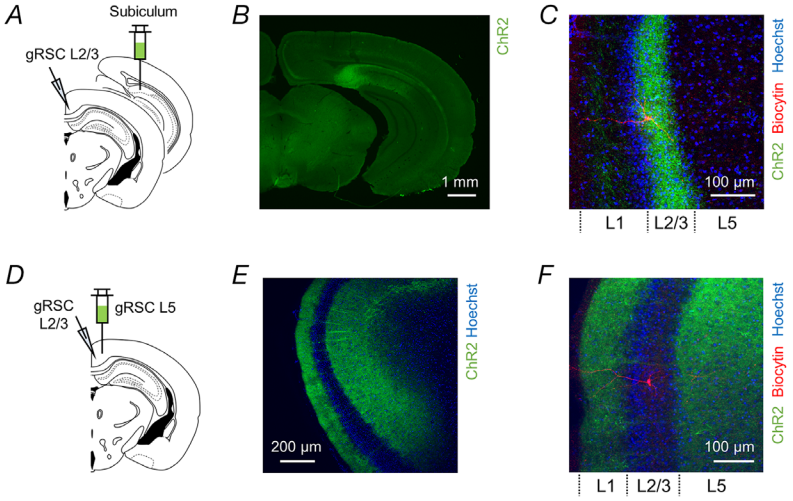

Figure 7. Injection of AAV5-CaMKII-ChR2-EYFP and patch-clamp recordings from gRSC L2/3 after ChR2 expression
A, schematic illustration of the sites of AAV5-CaMKII-ChR2-EYFP injection (subiculum) and whole-cell patch-clamp recordings (gRSC L2/3). *B*, representative image showing the expression of ChR2 at the injection site in the subiculum. *C*, representative confocal photographs of ChR2-EYFP fluorescence. ChR2-EYFP was observed in the gRSC L2/3 terminal field of subicular projections (green) and the patched neuron (red) in a Hoechst-counterstained section (blue). *D–F*, the same as *A–C* for AAV injection into gRSC L5. ChR2-EYFP expression was observed in gRSC L5 and L1. [Colour figure can be viewed at wileyonlinelibrary.com]

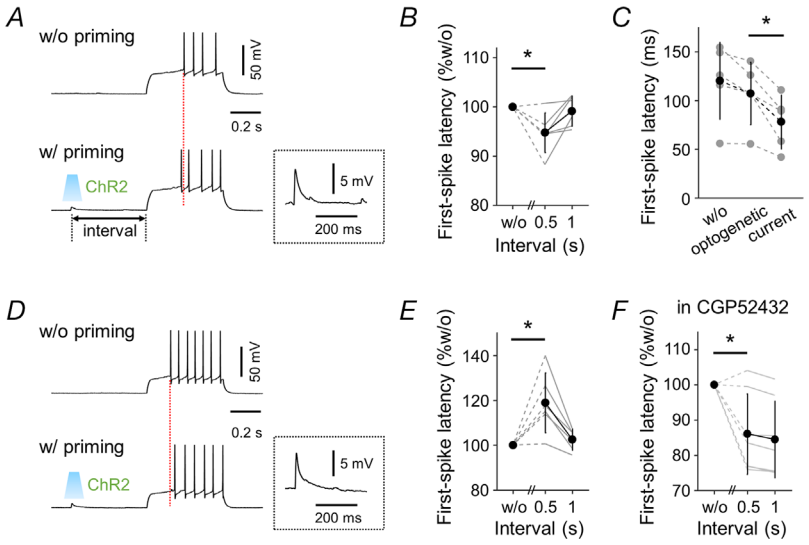

Figure 8. Optogenetic priming of afferents from the subiculum or gRSC L5 oppositely modulates the first-spike latencies of gRSC L2/3 neurons
A, optogenetic priming with a 2-ms blue light pulse to activate subicular inputs 500 ms before the current injection shortened the first-spike latencies in a gRSC L2/3 neuron. Top, an example trace without optical priming. Bottom, an example trace with a 2-ms optical priming stimulus delivered 500 ms before the main current injection. The light-evoked EPSP is magnified in the inset. *B*, the first-spike latencies are summarized for three conditions: without (w/o) priming and with priming by a blue light pulse at intervals of 500 and 1000 ms. The latencies were normalized to the average for w/o priming trials for each neuron. n = 6 cells from 5 mice, 10−14 trials for each interval. $^*P$ = 0.0241, t_5 = −3.1971, paired t test. *C*, comparison of first spike latency for trials without priming or with optogenetic priming or current injection priming. n = 5 cells from 3 mice. Each type of priming was performed 4−8 trials for each cell. $^*P$ = 0.0104, t_4 = 4.55, paired t test. *D* and *E*, the same as *A* and *B* for AAV injection into gRSC L5. First-spike latencies were delayed upon blue light priming at an interval of 500 ms compared to upon AAV injection into the subiculum. In *E*, n = 6 cells from 4 mice, 6–10 trials for each interval. $^*P$ = 0.0174, t_5 = 3.4938, paired t test. *F*, blue-light stimuli were applied to slices from mice that had received AAV injection into the gRSC L5, while CGP52432 was bath-applied at a concentration of 10 μM. n = 7 cells from 5 mice, 10–11 trials for each interval. $^*P = 1.8\times10^{-2}$, t_6 = −3.23, paired t test. [Colour figure can be viewed at wileyonlinelibrary.com]

to current injection. In the other four types of pyramidal cells tested, the same protocols caused the opposite effects: prior depolarization retarded the generation of the first action potential. In general, neurons function homeostatically or adaptively through feedback inhibition. A typical example is spike-frequency adaptation, a progressive reduction in action potential frequencies during an extended period of depolarization, which may be mediated by calcium-activated potassium or chloride channels (Ha & Cheong, 2017). This process enables the neuron to respond selectively to stronger inputs, filtering the information it receives from other neurons. Desensitization in gRSC L5, ACC L2/3, hippocampal CA1 and PRC L6 neurons represents

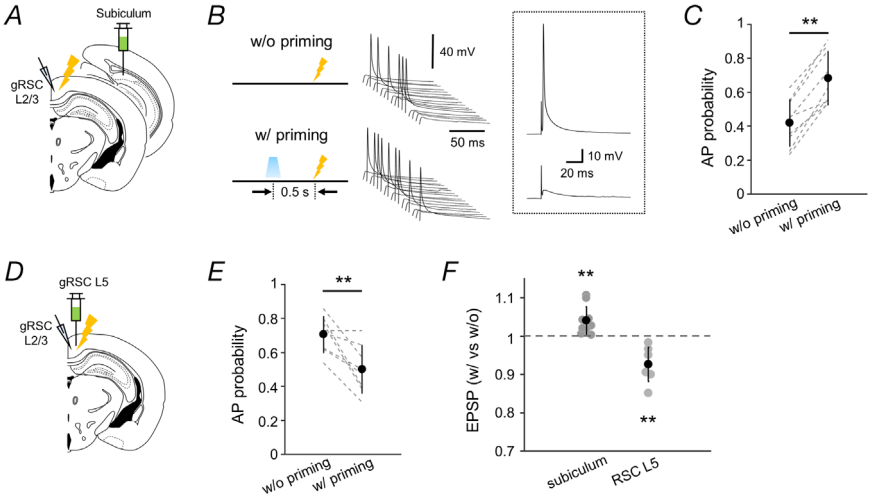

Figure 9. Optogenetic priming of the subiculum, but not gRSC L5, increases the firing probabilities and EPSP amplitudes of gRSC L2/3 neurons
A, schematic illustration of the sites of AAV5-CaMKII-ChR2-EYFP injection (subiculum), whole-cell patch-clamp recordings (gRSC L2/3), and extracellular electrical stimulation (gRSC L2/3 was deeper than the patch-clamp site). *B*, left: experimental design of a w/o priming trial (top) and a w/ priming trial (bottom). In the w/ priming trial, a 2-ms blue light pulse was delivered 500 ms before extracellular electrical stimulation. The strength of the electrical stimulation was set to induce an action potential in gRSC L2/3 neurons at a moderate probability of approximately 40%. *B*, right: responses of a gRSC L2/3 neuron to electrical stimulation in w/o and w/ priming trials (alternating, 17 of each type). Representative trials with (top) and without (bottom) an action potential are magnified in the inset. *C*, the firing probabilities in 11–18 w/o and w/ priming trials for 9 cells from 7 mice are summarized. $^{**}P = 2.3 \times 10^{-5}$, $t_8 = 8.71$, paired *t* test. *D* and *E*, the same as *A* and *C* but for AAV injection into the gRSC L5. $n = 10–21$ trials for 8 cells from 6 mice. $^{**}P = 5.2 \times 10^{-3}$, $t_7 = 3.99$, paired *t* test. *F*, priming-induced changes in the amplitudes of EPSPs evoked by subthreshold electrical stimulation. Data were obtained from 10 and 7 neurons from 8 and 5 mice injected with AAV into the subiculum and the gRSC L5, respectively (10–15 and 8–12 trials each). The error bars represent the SDs. $^{**}P < 0.001$ *versus* 1, bootstrap test for means.
[Colour figure can be viewed at wileyonlinelibrary.com]

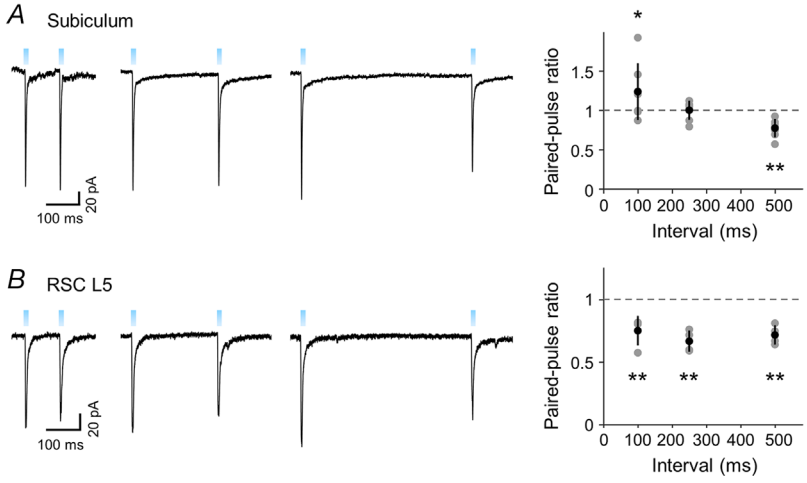

Figure 10. Paired-pulse light stimulation fails to induce synaptic facilitation
A, left: representative traces of voltage-clamp recordings from gRSC L2/3 neurons in response to paired-pulse blue light stimulation at interstimulation intervals of 100, 250 and 500 ms in a brain slice prepared from a mouse that had received AAV injection into the subiculum. *A*, right: summary of paired-pulse ratios in 7 cells from 4 mice. $^{*}P = 0.011$ *versus* 1 for 100 ms, $P = 0.47$ for 250 ms and $^{**}P < 0.001$ for 500 ms, bootstrap test for means. *B*, the same as *A* but in slices prepared from mice that received AAV injection into the gRSC L5. $n = 4$ cells from 2 mice. $^{**}P < 0.001$ for 100, 250 and 500 ms. [Colour figure can be viewed at wileyonlinelibrary.com]

a similar adaptation, emphasizing the sensitization observed in gRSC L2/3 neurons as an exceptional property. Because paired-pulse stimulation did not apparently facilitate the second EPSCs in gRSC L2/3 neurons, the facilitatory priming effect is likely to depend on postsynaptic mechanisms. One possible mechanism is the involvement of calcium-activated ion channels in gRSC L2/3 late-spiking neurons, such as BK ('big potassium') channels, which are gated by depolarization and increased intracellular calcium concentrations, and ANO2 (anoctamin 2) channels, which mediate chloride ion influx in hippocampal neurons (Huang *et al.* 2012) and the cerebral cortex (Vocke *et al.* 2013). Both types of ion channels are known to modulate the process of spike-frequency adaptation. In gRSC L2/3 late-spiking neurons, the extent of spike-frequency adaptation was much smaller than that observed in regular-spiking cells (Kurotani *et al.* 2013), suggesting that gRSC L2/3 neurons have a lower level of expression of BK and ANO2 channels. Thus, unlike that of other cells, the membrane excitability of gRSC L2/3 late-spiking neurons may not be decreased by prior depolarization. These channels modulate membrane excitability and action potential timing by interacting with Kv1.1, Kv1.4, and Kv4.3, which shape the late-spiking properties of gRSC L2/3 neurons (Kurotani *et al.* 2013). In the present study, we found that Kv1 channels seem to contribute, at least in part, to the priming effect based on pharmacological experiments utilizing DTX-K. It is possible that either the blockage of other subtypes of Kv channels or the application of higher concentration of DTX-K completely abolishes the priming effects. Some Kv channels are known to be differentially activated by repetitive depolarizing stimuli. For example, in response to a double-pulse protocol, activation kinetics of Kv1.2 during the second pulse was accelerated (Rezazadeh *et al.* 2007), whereas Kv1.4 currents tended to become inactivated, and the complete recovery may need up to several seconds, possibly modulated by CaMKII phosphorylation (Roeper *et al.* 1997). Distinct expression levels of Kv channels in gRSC L2/3 neurons may cause a difference in the intensity of K^+ efflux in response to repetitive depolarization based on their inactivation properties, thereby resulting in the unique facilitatory priming effect. Meanwhile, in our experiments, the baseline membrane potential was not significantly altered before the priming stimulus and the main stimulus. This may be regulated by activity of multiple subtypes of Kv channels or other potassium channels, including Ca^{2+}-activated K^+ (K_{Ca}) channels regulated by $[Ca^{2+}]_i$ residues. Further research on the influence of the priming stimulation or repetitive stimuli on Kv1 currents and possible involvements of other types of Kv channels that are highly expressed in gRSC L2/3 remain necessary.

We demonstrated that prior activation of subicular inputs shortened the first-spike latency and increased

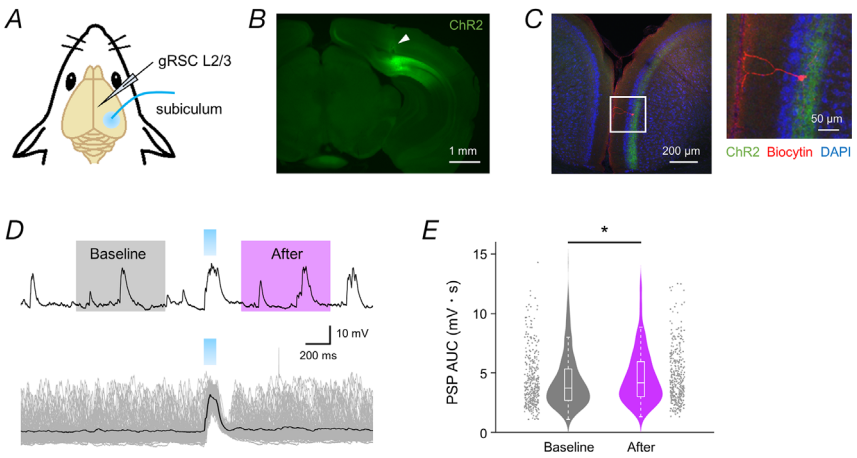

Figure 11. Activation of the subiculum increases subsequent spontaneous PSPs in gRSC L2/3 *in vivo*
A, schematic illustration of *in vivo* whole-cell patch-clamp recording from a gRSC L2/3 neuron in an anaesthetized mouse that had received injection of AAV5-CaMKII-ChR2-EYFP into the subiculum and blue light stimulation of the subiculum through an optic fibre. *B*, a confocal image showing ChR2-EYFP fluorescence and an optic fibre track (white arrowhead) in a coronal brain section. *C*, biocytin-based *post hoc* visualization of a patched gRSC L2/3 pyramidal cell in DAPI-counterstained slices from the same mouse, as shown in *B*. *D*, top: a representative membrane potential trace of the neuron shown in *C* before and after 100-ms blue light stimulation of the subiculum. The charges of spontaneous PSPs (the area under the curve) were measured for two 700-ms periods before (baseline) and after a light stimulus (−1.0 to −0.3 s and 0.3-1.0 s relative to the stimulus onset). *D*, bottom: the average response (black) of a total of 120 consecutive trials (grey) in the same cell, as shown in the top panel in *D*. *E*, the EPSP charges are compared between before (baseline) or after the light stimuli. n = 380 trials in 5 cells (5−135 trials each) in 5 mice. $^*P = 3.4 \times 10^{-2}$, $t_{758} = 2.12$, Student's t test. [Colour figure can be viewed at wileyonlinelibrary.com]

the firing probability of gRSC L2/3 neurons, whereas activating gRSC L5 inputs exerted the opposite effects. Subicular projections are reported to excite the somata of gRSC L2/3 neurons via vGlut1- or vGlut2-expressing bursty pyramidal cells (Yamawaki *et al*. 2019*a*). Thus, our somatic current injection might mimic somatic inputs from bursty pyramidal cells. Under our experimental conditions, optogenetic activation of subicular inputs did not induce an action potential in gRSC L2/3 neurons, but gRSC L2/3 neurons were significantly sensitized.

Optogenetic stimulation of gRSC L5 inputs elicited EPSPs in gRSC L2/3 neurons, but it did not facilitate the responses of the neurons to subsequent current injection or synaptic activation. The facilitatory effect of gRSC L5 priming was observed only when $GABA_B$ receptors were inhibited. $GABA_B$ receptor-mediated feedforward inhibition is widely found in the cerebral cortex and regulates cortical microcircuit operation (Isaacson & Scanziani, 2011). Therefore, gRSC L5 neurons probably recruited some class of inhibitory interneurons and masked the facilitatory priming effect via $GABA_B$ receptor-mediated feedforward inhibition. For instance, gRSC L2/3 late-spiking neurons frequently receive inhibitory inputs from neighbouring fast-spiking interneurons, suggesting that gRSC L2/3 involves an inhibition-dominated network containing predominantly feedforward inhibition (Brennan *et al*. 2020). Another explanation is that ongoing background activity of $GABA_B$ receptors masked the effect of gRSC L5 priming independently of feedforward inhibition. Based on our results, excitatory projections from the subiculum directly target and excite the somata of gRSC L2/3 neurons, while excitatory inputs from gRSC L5 possibly modulate L2/3 neurons via dendrites that extend into L1. Because the process of activating gRSC L2/3 neurons differs under the two conditions, the extent of influence by $GABA_B$ activity may also differ due to dendritic inhibition mediated by $GABA_B$ receptors (Tamás *et al*. 2003).

The subiculum is anatomically related to the hippocampus and constitutes a relay point between the hippocampus and the gRSC. In the present research, we observed increased excitability of gRSC L2/3 neurons following the activation of subicular inputs based on *in vivo* patch clamp recordings, which was probably generated by the activity of Kv1 channels. Hippocampal SWRs increase neuronal activity in gRSC L2/3 (itzan *et al*. 2020), whereas gRSC L5 neurons receive inhibitory projections from the hippocampus (Yamawaki *et al*. 2019*b*) and are likely to be suppressed after hippocampal SWRs (Opalka *et al*. 2020). Hippocampal SWRs represent synchronized activity of hippocampal neuron populations and are strong candidates for the synchronization of subicular activity, which resembles optogenetic activation of the subiculum. Therefore, it is possible that hippocampal SWRs induce the responsiveness of gRSC L2/3 neurons. Although inhibitory neurons in the gRSC also exhibit associated responses to hippocampal SWRs (Nitzan *et al*. 2020; Opalka *et al*. 2020), no direct evidence suggested that the overall activity of gRSC L2/3 neurons was suppressed via these inhibitory neurons. In contrast, gRSC L2/3 pyramidal cells mostly exhibit rapid increases in unit responses to SWRs (Nitzan *et al*. 2020). Because the gRSC is a brain network hub, hippocampal SWRs may facilitate information transmission through the gRSC. Moreover, because SWRs often emerge as consecutive chains of multiple SWRs that persist for hundreds of milliseconds (Davidson *et al*. 2009), the unique properties of gRSC L2/3 neurons may allow them to respond more sensitively to multiple SWR chains and facilitate the propagation of hippocampal SWRs to the neocortex, contributing to memory consolidation.

References

Alexander AS & Nitz DA (2015). Retrosplenial cortex maps the conjunction of internal and external spaces. *Nat Neurosci* **18**, 1143–1151.

Alexander AS & Nitz DA (2017). Spatially periodic activation patterns of retrosplenial cortex encode route sub-spaces and distance traveled. *Curr Biol* **27**, 1551–1560.e4.

Brennan EKW, Sudhakar SK, Jedrasiak-Cape I, John TT & Ahmed OJ (2020). Hyperexcitable neurons enable precise and persistent information encoding in the superficial retrosplenial cortex. *Cell Rep* **30**, 1598–1612.e8.

Cembrowski MS, Phillips MG, DiLisio SF, Shields BC, Winnubst J, Chandrashekar J, Bas E & Spruston N (2018). Dissociable structural and functional hippocampal outputs via distinct subiculum cell classes. *Cell* **173**, 1280–1292.e18.

Chase SM & Young ED (2007). First-spike latency information in single neurons increases when referenced to population onset. *Proc Natl Acad Sci U S A* **104**, 5175–5180.

Chen LL, Lin LH, Green EJ, Barnes CA & McNaughton BL (1994). Head-direction cells in the rat posterior cortex. I. Anatomical distribution and behavioral modulation. *Exp Brain Res* **101**, 8–23.

Corcoran KA, Donnan MD, Tronson NC, Guzmán YF, Gao C, Jovasevic V, Guedea AL & Radulovic J (2011). NMDA receptors in retrosplenial cortex are necessary for retrieval of recent and remote context fear memory. *J Neurosci* **31**, 11655–11659.

Czajkowski R, Jayaprakash B, Wiltgen B, Rogerson T, Guzman-Karlsson MC, Barth AL, Trachtenberg JT & Silva AJ (2014). Encoding and storage of spatial information in the retrosplenial cortex. *Proc Natl Acad Sci U S A* **111**, 8661–8666.

Davidson TJ, Kloosterman F & Wilson MA (2009). Hippocampal replay of extended experience. *Neuron* **63**, 497–507.

Funayama K, Minamisawa G, Matsumoto N, Ban H, Chan AW, Matsuki N, Murphy TH & Ikegaya Y (2015). Neocortical rebound depolarization enhances visual perception. *PLoS Biol* **13**, e1002231.

Gautrais J & Thorpe S (1998). Rate coding versus temporal order coding: a theoretical approach. *Biosystems* **48**, 57–65.
Ha GE & Cheong E (2017). Spike frequency adaptation in neurons of the central nervous system. *Exp Neurobiol* **26**, 179–185.
Hattori R, Danskin B, Babic Z, Mlynaryk N & Komiyama T (2019). Area-specificity and plasticity of history-dependent value coding during learning. *Cell* **177**, 1858–1872.e15.
Huang WC, Xiao S, Huang F, Harfe BD, Jan YN & Jan LY (2012). Calcium-activated chloride channels (CaCCs) regulate action potential and synaptic response in hippocampal neurons. *Neuron* **74**, 179–192.
Isaacson JS & Scanziani M (2011). How inhibition shapes cortical activity. *Neuron* **72**, 231–243.
Ishikawa D, Matsumoto N, Sakaguchi T, Matsuki N & Ikegaya Y (2014). Operant conditioning of synaptic and spiking activity patterns in single hippocampal neurons. *J Neurosci* **34**, 5044–5053.
Keene CS & Bucci DJ (2008). Contributions of the retrosplenial and posterior parietal cortices to cue-specific and contextual fear conditioning. *Behav Neurosci* **122**, 89–97.
Kurotani T, Miyashita T, Wintzer M, Konishi T, Sakai K, Ichinohe N & Rockland KS (2013). Pyramidal neurons in the superficial layers of rat retrosplenial cortex exhibit a late-spiking firing property. *Brain Struct Funct* **218**, 239–254.
Mao D, Kandler S, McNaughton BL & Bonin V (2017). Sparse orthogonal population representation of spatial context in the retrosplenial cortex. *Nat Commun* **8**, 243.
Nitzan N, McKenzie S, Beed P, English DF, Oldani S, Tukker JJ, Buzsáki G & Schmitz D (2020). Propagation of hippocampal ripples to the neocortex by way of a subiculum-retrosplenial pathway. *Nat Commun* **11**, 1947.
Nixima K, Okanoya K, Ichinohe N & Kurotani T (2017). Fast voltage-sensitive dye imaging of excitatory and inhibitory synaptic transmission in the rat granular retrosplenial cortex. *J Neurophysiol* **118**, 1784–1799.
Nixima K, Okanoya K & Kurotani T (2013). Current source-density analysis of intracortical circuit in the granular retrosplenial cortex of rats: a possible role in stimulus time buffering. *Neurosci Res* **76**, 52–57.
Opalka AN, Huang WQ, Liu J, Liang H & Wang DV (2020). Hippocampal ripple coordinates retrosplenial inhibitory neurons during slow-wave sleep. *Cell Rep* **30**, 432–441.e433.
Rezazadeh S, Kurata HT, Claydon TW, Kehl SJ & Fedida D (2007). An activation gating switch in Kv1.2 is localized to a threonine residue in the S2-S3 linker. *Biophys J* **93**, 4173–4186.
Roeper J, Lorra C & Pongs O (1997). Frequency-dependent inactivation of mammalian A-type K^+ channel KV1.4 regulated by Ca^{2+}/calmodulin-dependent protein kinase. *J Neurosci* **17**, 3379–3391.
Tamás G, Lorincz A, Simon A & Szabadics J (2003). Identified sources and targets of slow inhibition in the neocortex. *Science* **299**, 1902–1905.
Vann SD, Aggleton JP & Maguire EA (2009). What does the retrosplenial cortex do? *Nat Rev Neurosci* **10**, 792–802.
Vann SD, Kristina Wilton LA, Muir JL & Aggleton JP (2003). Testing the importance of the caudal retrosplenial cortex for spatial memory in rats. *Behav Brain Res* **140**, 107–118.
Vocke K, Dauner K, Hahn A, Ulbrich A, Broecker J, Keller S, Frings S & Möhrlen F (2013). Calmodulin-dependent activation and inactivation of anoctamin calcium-gated chloride channels. *J Gen Physiol* **142**, 381–404.
Yamawaki N, Corcoran KA, Guedea AL, Shepherd GMG & Radulovic J (2019*a*). Differential contributions of glutamatergic hippocampal→retrosplenial cortical projections to the formation and persistence of context memories. *Cereb Cortex* **29**, 2728–2736.
Yamawaki N, Li X, Lambot L, Ren LY, Radulovic J & Shepherd GMG (2019*b*). Long-range inhibitory intersection of a retrosplenial thalamocortical circuit by apical tuft-targeting CA1 neurons. *Nat Neurosci* **22**, 618–626.

Additional information

Data availability statement

The data that support the findings of this study are available from the corresponding author upon reasonable request.

Competing interests

All authors declare that there are no conflicts of interest.

Author contributions

The study was performed in the Laboratory of Chemical Pharmacology, Graduate School of Pharmaceutical Sciences at The University of Tokyo. M.G. (first author) contributed to the conceptual design, data acquisition, analysis, interpretation and drafting/revising of the manuscript. A.N. (second author) contributed to the experimental works and interpretation of the data. Y.I. (corresponding author) contributed to the conceptual design, interpretation of the data and drafting/revising of the manuscript. All authors have approved the final version of the manuscript and agree to be accountable for all aspects of the work. All persons designated as authors qualify for authorship, and all those who qualify for authorship are listed.

Funding

This work was supported by JST ERATO (JPMJER1801), Institute of AI and Beyond of the University of Tokyo, and JSPS Grants-in-Aid for Scientific Research (18H05525).

Acknowledgements

We thank Dr Tohru Kurotani (National Center of Neurology and Psychiatry) for commenting on the experimental procedures.

Keywords

hippocampus, plasticity, retrosplenial cortex, sensitization, subiculum

Supporting information

Additional supporting information may be found online in the Supporting Information section at the end of the article.

Table S1. Fig. 4C z-score data
Table S2. Fig. 11E AUC data
Statistical Summary Document